A population-level model from the microscopic dynamics in Escherichia coli chemotaxis via Langevin approximation

He Zhuo-Ran(贺卓然)[a], Wu Tai-Lin(吴泰霖)[a], Ouyang Qi(欧阳颀)[a)b)†], and Tu Yu-Hai(涂豫海)[c]

[a] *State Key Laboratory for Mesoscopic Physics, School of Physics, Peking University, Beijing* 100871, *China*

[b] *Center for Theoretical Biology, Peking University, Beijing* 100871, *China*

[c] *IBM T. J. Watson Research Center, Yorktown Heights, New York* 10598, *USA*

(Received 6 April 2012; revised manuscript received 10 May 2012)

Recent extensive studies of Escherichia coli (E. coli) chemotaxis have achieved a deep understanding of its microscopic control dynamics. As a result, various quantitatively predictive models have been developed to describe the chemotactic behavior of E. coli motion. However, a population-level partial differential equation (PDE) that rationally incorporates such microscopic dynamics is still insufficient. Apart from the traditional Keller–Segel (K–S) equation, many existing population-level models developed from the microscopic dynamics are integro-PDEs. The difficulty comes mainly from cell tumbles which yield a velocity jumping process. Here, we propose a Langevin approximation method that avoids such a difficulty without appreciable loss of precision. The resulting model not only quantitatively reproduces the results of pathway-based single-cell simulators, but also provides new inside information on the mechanism of E. coli chemotaxis. Our study demonstrates a possible alternative in establishing a simple population-level model that allows for the complex microscopic mechanisms in bacterial chemotaxis.

Keywords: bacterial chemotaxis, population-level model, Langevin approximation

PACS: 87.17.Jj, 87.17.Aa, 87.18.Mp, 87.18.Vf **DOI:** 10.1088/1674-1056/21/9/098701

1. Introduction

The system of chemotactic signal transduction in bacterial Escherichia coli (E. coli) is one of the most widely studied biological systems. In this regulatory system, the relevant molecular players and their interactions in the chemotactic pathway have been identified, and the corresponding mathematical models[1] have been established, which can quantitatively describe the chemotactic behavior on cell level. However, the dynamic description on population level falls behind people's growing understanding of the microscopic pathway dynamics. This problem becomes more pronounced as new experimental conditions using microfluidic technology[2−4] put the assumptions of traditional population-level models into question. As a result, frequency-dependent chemotaxis behaviours[5] are discovered, which cannot be explained using traditional Keller–Segel (K–S) equation.

1.1. Traditional K–S equation

The most widely used partial differential equation (PDE) model at present is the Keller–Segel equation.[6] It is the first model of bacterial chemotaxis prior to any quantitative understanding of the underlying molecular regulatory pathway. Its general form[7] is given by (if ligand consumption, cell reproduction and death are ignored)

$$\frac{\partial p}{\partial t} = -\boldsymbol{\nabla}\cdot(p\chi(c)\boldsymbol{\nabla}c) + \boldsymbol{\nabla}\cdot(\mu(c)\boldsymbol{\nabla}p), \qquad (1)$$

where $p(\boldsymbol{r},t)$ is the population density, $c(\boldsymbol{r},t)$ is the predefined ligand concentration field, and the chemotactic factor $\chi(c)$ and the diffusion coefficient $\mu(c)$ are c-dependent parameters. The model assumes an instant sensing of the ligand gradient, in that the chemotactic drift velocity $\boldsymbol{v}_d = \chi(c)\boldsymbol{\nabla}c$ in the first term is determined by the instant gradient $\boldsymbol{\nabla}c$. This assumption is valid when the field variation is slow and the field gradient is mild. In these situations the K–S equation can successfully predict the cells' chemotactic behaviors on population level. However, under cer-

†Corresponding author. E-mail: qi@pku.edu.cn

© 2012 Chinese Physical Society and IOP Publishing Ltd

tain conditions, such as in a microfluidic device where the concentration field can vary sharply and quickly on a small length scale, the K–S equation fails because the above assumption is no longer valid. In order to develop a more general model, one has to look deeper into the chemotactic mechanisms on the microscopic scale, and develop a population-level model that incorporates such microscopic information.

1.2. Microscopic pathway dynamics

In wild environments, unicellular prokaryotes like E. coli are too small to sense any spatial difference in ligand concentration within cell length, and hence the only way they can achieve chemotaxis is through temporal comparison[8,9] of the concentrations they encounter. Every E. coli has a cluster of chemo-receptors to do the job. They bind with the ligand molecules (attractant) in a reversible biochemical reaction to measure the local concentration c. This information is passed on to the chemotactic control protein CheA. The activity $A(c,m)$ of kinase CheA on the receptors decreases with c and increases with the average methylation level m of the receptors. The latter follows the rise and fall of c (known as adaptation) due to two antagonistic enzymes CheB and CheR. The dynamics is governed by[10]

$$\frac{\mathrm{d}m}{\mathrm{d}t} = \dot{m}(A(c,m)) = \dot{m}(c,m). \tag{2}$$

The function $\dot{m}(A)$ monotonically decreases with A and has only one zero (denoted as A_0), ensuring a unique and stable fixed point $m_0(c)$ that rises with c. This dynamics makes m the recent past of c and A the temporal comparison of the ligand concentrations experienced by the cell. When $m_0(c) = m$, the kinase activity $A(c, m_0(c)) = A_0$ lies at a fixed median level independent of c, which is known as precise adaptation.[11] When $m_0(c) > m$, the concentration is on the rise, and thus activity $A < A_0$, otherwise $A \geq A_0$.

The signal stored in $A(c,m)$ controls the intracellular concentration of phosphorylated (activated) response regulator CheYp through rapid phosphoryl transfer.[12] The dynamics of CheY phosphorylation and CheYp dephosphorylation are much faster than methylation, so that the CheY response can be modeled as an instantaneous function

$$Y(c,m) = \frac{[\mathrm{CheYp}](A)}{[\mathrm{CheYp}](A_0)} = f(A), \tag{3}$$

where $f(A)$ is monotonically increasing to principally amplify the signal. The dimensionless CheYp level $Y(c,m)$ modulates the flagellar motors' switching probability between counter-clockwise and clockwise rotating states, and hence the tumbling frequency. In a chemoattractant field, an E. coli cell tumbles (changes its swimming direction suddenly) more frequently when $Y(c,m)$ is high, and less frequently when it is low. Consequently, the displacement on a longer time scale is larger up the gradient than down the gradient, and chemotaxis is achieved.

1.3. Why Langevin approximation

While the dependence of single flagellar switching probability on CheYp level is clearly studied,[13] it remains yet complicated how all the flagella together determine the tumble and run of the whole cell.[14] Moreover, based on the information available at present, exact methods treating tumbles as a velocity jumping process often yield an integro-PDE,[15,16] which usually not only defies further theoretical analysis, but also makes it difficult to include more realistic motility mechanisms into the model. Hence, the first step in our work is to remove these obstacles.

Our method is to apply a Langevin approximation to avoid dealing with a velocity jumping process. As a result, a new type of PDE is developed. This will be discussed in Section 2. In Section 3, the PDE's compatibility with the K–S equation under certain conditions is investigated theoretically. This analysis helps us understand the meanings of parameters $\chi(c)$ and $\mu(c)$ in the K–S model from the perspective of cell dynamics. In Section 4, the precision of our model is tested in two simulation situations where the K–S equation fails. Finally, the discussion Section addresses the advantages and drawbacks of our modeling approach compared with the work of others.

2. Building the PDE model

2.1. Langevin approximation in a fixed $Y(c, m)$ state

Let us first consider a simple case in which the methylation dynamics (Eq. (2)) is stopped, and hence m remains fixed. This can be experimentally realized by knocking out CheB and CheR. Suppose we put the cell in a uniform and stationary ligand concentration c on a two-dimensional (2D) plane so that the value of

$Y(c,m)$ is fixed according to Eq. (3). In this situation one will expect a fixed pattern of flagellar motion of the cell. The movement of the cell follows a random walk pattern, which can be modeled as a wide-sense stationary (WSS) stochastic process of the 2D swimming velocity $\boldsymbol{v}(t)$. The lower the value of $Y(c,m)$, the less frequently the cell tumbles, and thus the farther the cell travels in the random walk. However, notice that even in complete absence of tumbles, the cell will not move strictly along a straight line, because collisions with surrounding liquid molecules gradually and randomly change its swimming direction. This effect is known as rotational diffusion[17] and is usually modeled by an angular Wiener process

$$\begin{aligned} &x = v\cos\theta_v \,\mathrm{d}t, \quad y = v\sin\theta_v \,\mathrm{d}t, \\ &\mathrm{d}\theta_v = \sqrt{2Z_\theta}\,\mathrm{d}W_t, \end{aligned} \tag{4}$$

where v is the maximum swimming speed, typically 15–25 μm/s for E. coli chemotaxis, Z_θ is the angular diffusion coefficient, typically 0.05–0.2 rad^2/s, and W_t is the standard Wiener process.

The master equation of Eq. (4) is a Fokker–Planck equation, a closed-form PDE. However, at higher $Y(c,m)$ level, the cell starts to tumble, and $\boldsymbol{v}(t)$ becomes a jumping process, whose exact master equation has to be an integro-PDE (see Section 5), or even non-Markovian if the duration of tumbles is taken into consideration. However, since the WSS process $\boldsymbol{v}(t)$ is only short-term correlated, which means its second-order moment $\kappa(\tau) = \langle \boldsymbol{v}(t)\cdot\boldsymbol{v}(t+\tau)\rangle$ has an exponential tail, one can deduce the spatially diffusive long-term behavior from central limit theorem and calculate the diffusion coefficient

$$D(Y) = \lim_{t\to+\infty} \frac{1}{4t}\left\langle r^2(t)\right\rangle = \frac{1}{2}\int_0^{+\infty} \kappa(\tau)\,\mathrm{d}\tau. \tag{5}$$

Hence, as long as the cell tumbles very frequently and the steady-state diffusive behavior arises quickly, $D(Y)$ becomes almost the only determinant of the evolution of its probability distribution. We therefore have an idea of bridging the rare tumbling limit (Eq. (4)) and the frequent tumbling limit (Eq. (5)) with the following model:

$$\begin{aligned} &x = v\cos\theta_v \,\mathrm{d}t, \quad y = v\sin\theta_v \,\mathrm{d}t, \\ &\mathrm{d}\theta_v = \sqrt{2Z_{\mathrm{eff}}(Y)}\,\mathrm{d}W_t, \end{aligned} \tag{6}$$

where the parameter $Z_{\mathrm{eff}}(Y)$ is properly set so that the long-term diffusion coefficient

$$D(Y) = \frac{v^2}{2Z_{\mathrm{eff}}(Y)} \tag{7}$$

derived from the temporal autocorrelation function $\kappa(\tau) = v^2\exp(-Z_{\mathrm{eff}}\tau)$ of the model given by Eq. (6) agrees with the real process $\boldsymbol{v}(t)$ in all $Y(c,m)$ states. In this way we can aggregate the effects of all existing motility mechanisms, including tumbling, speed changing, multi-flagella switching, auxiliary navigation,[18] and many yet unknown details, into a $Z_{\mathrm{eff}}(Y)$-modulated equivalent angular Wiener process. The validity of such mechanism aggregation is our first major assumption, which is defined as the Langevin approximation.

2.2. Generalizing to a spatiotemporal concentration field

In a spatiotemporal concentration field and with methylation dynamics (Eq. (2)) turned on, we assume that the $Y(c,m)$ value of each cell varies in a quasi-static manner so that equation (6) still holds. This means no substantial change in Z_{eff} occurs within the correlation time $\tau_{\mathrm{c}} = 1/Z_{\mathrm{eff}}$ of $\kappa(\tau)$, which is roughly the duration of a running period between two tumbles. With this second assumption, in a 2D concentration field $c(\boldsymbol{r},t)$ of an inconsumable ligand, we may put Eqs. (2), (3), and (6) together to form a Langevin equation and then derive the corresponding Fokker-Planck equation as the population-level PDE

$$\begin{aligned} &\frac{\partial P}{\partial t} + \frac{\partial}{\partial m}\left[\dot{m}(A(c,m))P\right] + \boldsymbol{v}(\theta_v)\cdot\boldsymbol{\nabla}P \\ &= Z_{\mathrm{eff}}(Y(c,m))\frac{\partial^2 P}{\partial\theta_v^2}, \end{aligned} \tag{8}$$

where

$$\boldsymbol{v}(\theta_v) = v\boldsymbol{e}_x\cos\theta_v + v\boldsymbol{e}_y\sin\theta_v,$$

and $P(\boldsymbol{r},m,\theta_v,t)$ is the probability density of a single cell at time t, also proportional to the population density in absence of cell–cell interaction and population heterogeneity. Cell reproduction and death are also ignored. By connecting the $\dot{m}(A)$ form (Eq. (2)) with the $Z_{\mathrm{eff}}(Y)$ form (Eqs. (5) and (7)), equation (8) provides a PDE model without the integral term in velocity jumping.

2.3. Meaning of $Z_{\mathrm{eff}}(Y)$

The newly introduced model parameter $Z_{\mathrm{eff}}(Y)$ determined by Eqs. (5) and (7) can be understood as an effective tumbling frequency that characterizes the randomness of cell motion at different $Y(c,m)$ levels. We may theoretically calculate it in a simple motility model at a fixed $Y(c,m)$ level. In this process we can

illustrate its meaning and how it aggregates different mechanisms into a number.

Consider a cell swimming at constant speed v (except when tumbling) undergoing rotational diffusion of coefficient Z_θ. Every running period is determined by the duration between adjacent tumble events, which is exponentially distributed with a mean time $\tau_{\rm run}(Y)$. Every tumble halts the cell for some arbitrarily distributed time with a mean time $\tau_{\rm tumble}(Y)$, during which it swerves by an angle $\theta\in[-\pi,\pi]$ governed by a symmetric probability distribution $p(\theta|Y)$ with remaining correlation $\langle\cos\theta\rangle_Y=\alpha(Y)$. From the derivation in Appendix A, we have

$$Z_{\rm eff}(Y)=\left(\frac{1-\alpha(Y)}{\tau_{\rm run}(Y)}+Z_\theta\right)\left(1+\frac{\tau_{\rm tumble}(Y)}{\tau_{\rm run}(Y)}\right), \quad (9)$$

where $\tau_{\rm run}(Y)$, $\tau_{\rm tumble}(Y)$, and $\alpha(Y)$ can be measured by tracing single cells experimentally.[14,17]

Equation (9) shows clearly how mechanism aggregation is done. If tumbles take no time, $Z_{\rm eff}$ is the total effect of rotational diffusion Z_θ and a Poisson tumbling process of frequency $1/\tau_{\rm run}$ with remaining correlation α (the correlation between velocities before and after the tumble). Such a correlation makes one such tumble be equivalent to only $1-\alpha$ ideal tumbles with no correlation. This gives $Z_{\rm eff}$ the name "effective tumbling frequency". The effects of tumbles and rotational diffusion are added up in the sense that they both decorrelate $\boldsymbol{v}(t)$ from its past by introducing randomness, though in different ways. The $Z_{\rm eff}$ increases with $\tau_{\rm tumble}$ because a longer rest time is equivalent to a higher tumbling frequency in reducing the diffusion coefficient $D(Y)$.

2.4. Obtaining $Z_{\rm eff}(Y)$ in simulations

The above simplified analysis neglects the transitions between tumbles and runs, so it does not work well at high $Y(c,m)$ when such transitions happen frequently. Neither does it consider multi-flagella switching and other memories that may make the running period distribution deviate from exponential. In general, an analytical form of $Z_{\rm eff}(Y)$ is difficult to develop if one considers all the detailed dynamics of tumbles. A more convenient way is to measure the diffusion coefficient $D(Y)$ directly in simulations or experiments. The $Z_{\rm eff}(Y)$ curve can then be calculated using Eq. (7). Figure 1 shows the results of such simulations using pathway-based single-cell simulators, RapidCell[19] and SPECS[20], with theoretical results derived from Eq. (9) superimposed for comparison. Experimental curves can, in principle, be measured in the same way.

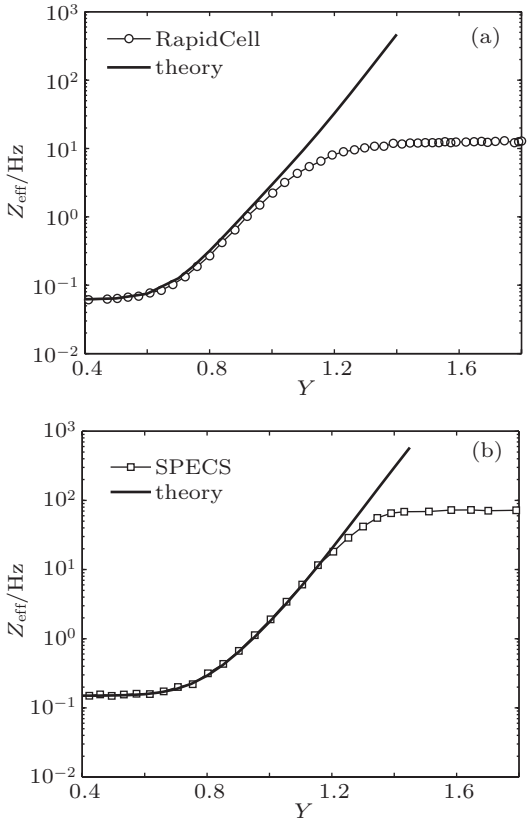


Fig. 1. $Z_{\rm eff}(Y)$ curves in theory (Eq. (9)) and simulations using (a) RapidCell (ver. 1.2.3) and (b) SPECS. Functions $\tau_{\rm run}(Y)$, $\tau_{\rm tumble}(Y)$, and $\alpha(Y)$ are set in accordance with the simulators. All adjustable parameters in the simulators assume default values that are the same as in Refs. [19] and [20]. In the cell motion part of RapidCell, the "voting motors" model is replaced with a more advanced "distortion factor" model.[21]

The S-shaped $Z_{\rm eff}(Y)$ curves of both two simulators agree with the simplified theoretical model when Y is low. When $Y<0.6$, the $Z_{\rm eff}(Y)$ tends to reach a constant, the rotational diffusion coefficient Z_θ. This corresponds to the situation where m is far below $m_0(c)$, so that $\tau_{\rm run}(Y)\to\infty$ and the cell runs for most of the time. Therefore, its swimming direction only gradually changes due to rotational diffusion. At higher Y level, the $Z_{\rm eff}(Y)$ rises above the lower plateau Z_θ and starts to grow exponentially fast around $Y=1$, namely the usual CheYp level due to adaptation. This illustrates the high sensitivity of E. coli's chemotactic system: a small change in Y determined by the temporal comparison of ligand concentrations can lead to a dramatic change in the effective tumbling frequency $Z_{\rm eff}(Y)$.

Far above $Y = 1$, however, the growth of $Z_{\rm eff}(Y)$ in simulations slows down as it asymptotically attains another plateau, which cannot be explained by the simplified theoretical model in Eq. (9). This discrepancy is mainly caused by the run-tumble transitions. When $Y > 1.4$, for instance, the running periods are extremely short so that $\tau_{\rm run}(Y) \to 0$. Consequently, the cell spends most of the time tumbling and going through transitions between tumble and run states. Cell motion during such transitions makes the diffusion coefficient $D(Y)$ nonzero and $Z_{\rm eff}(Y)$ bounded. The theoretical $Z_{\rm eff}(Y)$ determined by Eq. (9), neglecting such transitions, impractically diverges to infinity.

3. Translating our PDE into the K–S equation

With $Z_{\rm eff}(Y)$ collecting all the microscopic motility mechanisms, we can quantitatively deduce the population-level chemotaxis from our model PDE (Eq. (8)). As an example, we will derive the classical K–S equation (Eq. (1)) from Eq. (8) in diffusion limit followed by rapid methylation limit (instant gradient sensing). By doing this, we can obtain some microscopic understandings of the population-level parameters $\chi(c)$ and $\mu(c)$ in the K–S equation. The derivation is sketched below.

First, we take the diffusion limit, i.e., the frequent tumbling limit at constant diffusion coefficient (swimming speed v also goes to infinity in compensation). This changes Eq. (8) into

$$\frac{\partial p}{\partial t} + \frac{\partial}{\partial m}\left[\dot{m}(A(c,m))p\right] = \boldsymbol{\nabla}\cdot\left[D(Y(c,m))\boldsymbol{\nabla}p\right], \quad (10)$$

where $\dot{m}(A(c,m))$, $Y(c,m)$, and $D(Y)$ are the same as those in Eqs. (2), (3), and (7). The new density $p(\boldsymbol{r}, m, t)$ no longer depends on θ_v since frequent tumbles make P almost uniform in θ_v.

Then we take the rapid methylation limit. By doing so, the probability density $p(\boldsymbol{r}, m, t)$ becomes concentrated at $m = m_0(c(\boldsymbol{r}, t))$, leading to a Dirac-delta function. Equation (10) further reduces exactly to the K–S equation (Eq. (1)), where the chemotactic factor $\chi(c)$ and the diffusion coefficient $\mu(c)$ are given by

$$\begin{aligned} \chi(c) &= \left.\frac{\partial D(c,m)}{\partial c}\right|_{m=m_0(c)}, \\ \mu(c) &= D(c, m_0(c)) = \text{const}. \end{aligned} \quad (11)$$

The expression of $\chi(c)$, together with Eq. (7), provides a clear insight into how the population-level chemotactic drift velocity $\boldsymbol{v}_{\rm d} = \chi(c)\boldsymbol{\nabla}c$ is related to the single-cell motion characterized by $Z_{\rm eff}(Y)$, provided that the two limits are good approximations. The expression $\mu(c)$=const is a natural result derived from our PDE based on precise adaptation. It was also a common assumption among early theoreticians on the K–S equation before precise adaptation was understood.[7] More detailed derivations of Eqs. (10) and (11) can be found in Appendix B.

4. Testing the PDE in simulations

We have shown that our PDE has good compatibility with the K–S equation under certain mild conditions. To further test its general validity, here we deliberately choose those cases where the K–S equation fails. Two situations are selected in this context: ring formation in a uniform and stationary concentration, and negative chemotaxis in a rapidly oscillating uniform gradient. We compare the simulation results of our PDE with RapidCell and SPECS.

Notice that both simulators allow for rotational diffusion, so both of their $Z_{\rm eff}(Y)$ curves (see Fig. 1) have a nonzero lower bound as the rare tumbling limit ($Y < 0.7$), where rotational diffusion dominates. Within this range, equation (6) is accurate, as the rotational diffusion is precisely modeled by an angular Wiener process. In the other end, when $Y > 0.9$, $Z_{\rm eff}(Y) > 1$ Hz, the steady-state diffusive behavior emerges in one second. This ensures the accuracy of Eq. (6) again, as it agrees with the real $\boldsymbol{v}(t)$ in long-term diffusion coefficient for all Y. Therefore, the only possible problematic range of Y is in the middle range, i.e., around 0.8, where neither does rotational diffusion perfectly dominate, nor does the steady-state diffusive behavior come soon enough. Thus, it is necessary to test our first modeling assumption, i.e., the Langevin approximation assumption, by investigating the case of $Y = 0.8$ in simulations. This happens to yield an anomalous phenomenon that the K–S equation cannot explain, namely, ring formation.

4.1. Ring formation in a uniform and stationary concentration

In a spatially uniform and temporally stationary concentration field c, we put $N = 20000$ bacte-

ria with the same swimming speed $v = 20$ μm/s and fixed methylation level m (by knocking out CheB and CheR) at the origin and $t = 0$. The initial velocity distribution is isotropic and the CheYp level of the cells is $Y(c, m) = 0.8$. Results of cell density evolution by our PDE and RapidCell are shown in Fig. 2.

From Fig. 2, one observes that a ring is clearly formed at $t = 2$ s after the cells set out from the origin heading toward their individual directions. At $t = 5$ s, as the ring expands outward, it becomes blurry since more and more cells lose their initial directions through tumbling and rotational diffusion; they thus get left behind inside the expanding frontier. At $t = 10$ s, the ring completely disappears as the steady-state diffusive behavior emerges. The formation of the ring, though seemingly easy to understand, is beyond the K–S equation which predicts only the diffusive behavior from the very beginning according to Eq. (1).

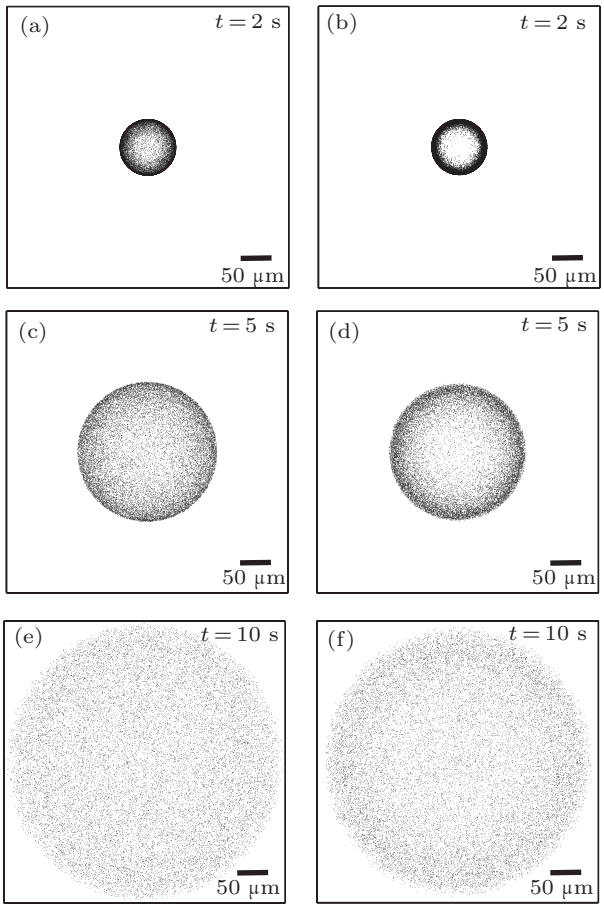


Fig. 2. Simulation results of the ring formation phenomenon by our PDE ((b), (d), and (f)) and RapidCell ((a), (c), and (e)) at $Y = 0.8$. The simulation is performed using the equivalent Langevin equation (Eq. (6)) of our PDE (Eq. (8)). Model parameters for RapidCell are the same as those in Fig. 1.

The simulation results do show some discernible discrepancy: at $t = 2$ s the result by our PDE apparently shows fewer cells inside the ring. This is mainly because in only 2 s, pure rotational diffusion makes large deflection angles impossible, but tumbles with a low probability, which enables such large deflection angles once tumbles really happen. However, the difference quickly disappears when $t = 5$ s, and the qualitative and overall pictures of ring formation and destruction are still satisfactorily captured. More simulation results reveal that if Y is set out of 0.7–0.9, no discrepancy can be observed at all, which is consistent with our previous discussion. Similar result is obtained using SPECS. Considering the variety of multi-flagellar motility mechanisms RapidCell incorporates, this part of simulation greatly supports our first modeling assumption.

4.2. Negative chemotaxis in a rapidly oscillating uniform ligand gradient

We now test our second modeling assumption: the quasi-static variation of $Y(c,m)$ states. In this case, the methylation dynamics (Eq. (2)) is turned on and cells are placed in a one-dimensional (1D) spatiotemporal concentration field $c(x, t) = 500 + x \sin(2\pi t/T)$ (μmol/L) (x in μm) on a 2D plane. It is a sinusoidally seesawing uniform-gradient field of MeAsp (an inconsumable chemoattractant) with tunable oscillation period T established within a finite microfluidic tube [−400 μm, 400 μm]. This situation resembles the experimental setup in a recent microfluidic experiment.[5] However, to simplify the calculation, reflective boundaries at both ends are applied in simulations, which is slightly different from the open boundary conditions used in that experiment. At different periods T we investigate how the "center of mass" $x_c(t)$ of the whole bacterial population changes as a function of time using RapidCell and SPECS, and compare the results with our PDE model's predictions. Figure 3 shows the results at $T = 200$ s.

As shown in Fig. 3, when the gradient oscillates at a frequency as fast as $1/200$ s$^{-1} = 5$ mHz, the extrema of $x_c(t)$ lag behind the zeroes of the gradient by about 15 s according to RapidCell, and about 30 s according to SPECS, during which time the centroid virtually moves against the gradient. Thus, the population exhibits negative chemotaxis as if it has inertia. This phenomenon, according to the short proof in Appendix C, is impossible for the K–S equation, albeit of the rapid oscillation. By comparison, our PDE model still successfully reproduces it accurately. This means

even in an oscillating field fast enough to induce negative chemotaxis, the quasi-static assumption is still valid.

We may set the oscillation period T in a wide range of different values to further test the assumption. Results are shown in Fig. 4, which records the amplitude of the centroid motion $x_c(t)$ and the phase lag of centroid velocity $v_c(t)$ at each driving period T. Figure 4 is qualitatively consistent with experimental results.[5] The good agreement between both simulators and our PDE model greatly corroborates the second assumption.

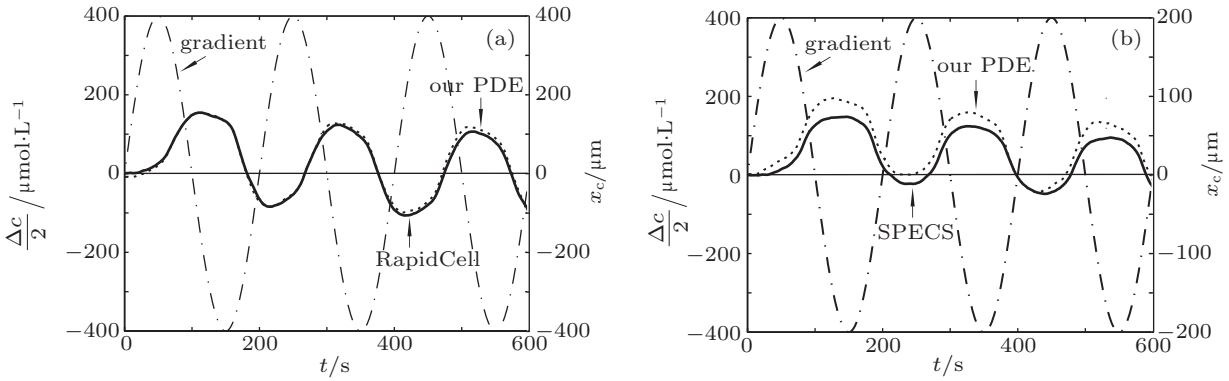


Fig. 3. Negative chemotaxis by our PDE compared with (a) RapidCell and (b) SPECS. The gradient line records half the difference of concentrations at the two ends of the tube [−400 μm, 400 μm]. Before the oscillation begins, all cells are fully adapted to the uniform concentration of 500 μmol/L. The simulation is done based on the equivalent Langevin equations (Eqs. (2), (3), and (6)) of our PDE. Model parameters for RapidCell and SPECS are the same as those in Fig. 1.

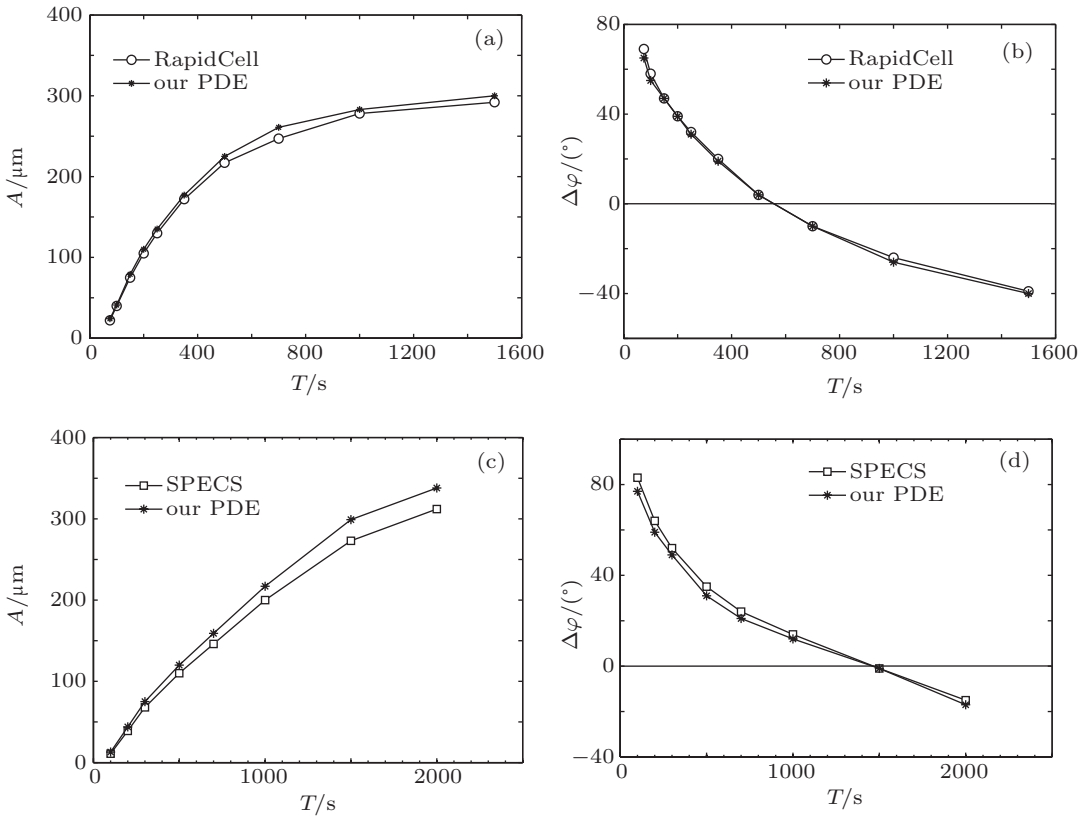


Fig. 4. Steady-state amplitude-period and phase-period curves. In (a) and (c), the amplitude A is defined by half the peak-to-peak value of $x_c(t)$. In (b) and (d), $\Delta\varphi$ is the phase angle by which the centroid velocity $v_c(t)$ lags behind the gradient determined by sinusoidal fitting of $x_c(t)$ (though the actual wave forms can have tilted or flat peaks). Model parameters in RapidCell and SPECS are the same as in Fig. 1.

5. Discussion

We have established a population-level PDE of *E. coli* chemotaxis, which describes how the bacterial population density evolves with time in a spatiotemporal concentration field. It complies with the major pathway dynamics $\dot{m}(A)$, $A(c,m)$, and $Y(A)$ of bacteria's adaptation and response to the time-varying concentration field. Downstream CheYp, everything is simplified to be an angular Wiener process with a state-dependent model parameter $Z_{\rm eff}(Y)$ to avoid dealing with a velocity jumping process. Using the $Z_{\rm eff}(Y)$ curve, we can deduce the population-level chemotactic behavior from our PDE by deriving the K–S equation and its model parameters $\chi(c)$ and $\mu(c)$ in certain limits. Though our PDE is only an approximate model, it keeps good accuracy in more general cases where the K–S equation may not work. This facilitates further population-level analysis of some new phenomena that cannot be explained by the K–S equation.

Compared with the work of other researchers in multi-scale modeling of bacterial chemotaxis, our model differs mainly in that it cannot discern individual tumbles, and thus the Langevin treatment becomes possible. As pointed out in Schnitzer's general theory of continuum random walk[15] with a "collision rate" (tumbling frequency) depending continuously on the direction of motion (with respect to ligand gradient), neither Langevin approach nor lattice method can treat such stochastic process exactly. As a result, the Smoluchowski equation (a type of integro-PDE) becomes almost the only choice. The complex mathematical form forbids non-ideal tumbles to be discussed. Such tumbles take non-ignorable time, slow down the swimming speed before and after them, and leave some remaining correlation between the new and old velocities. In some situations, there will be no choice but to ignore certain complex multi-flagella switching mechanisms, such as auxiliary navigation,[18] just because they are too hard to deal with mathematically. Our model, however, offers an alternative. Though not discerning individual tumbles definitely costs some precision (as discussed in Section 4.1), the simpler mathematical structure we obtain in return enables more realistic motility mechanisms to be included by incorporating all effects into $Z_{\rm eff}(Y)$.

It is possible to further simplify our PDE. In the original work of Erban and Othmer, a simple hyperbolic chemotaxis equation was derived from a velocity-jumping integro-PDE by using moment cloture.[22] Their equation makes an important correction to the K–S equation based on the assumption that the methylation level m is always distributed close to m_0, or at least has a negligible variance to enable a mean-field approximation. However, such an approximation is no longer valid in a spatiotemporal field in recently-developed microfluidic devices, where the ligand concentration can vary sharply and rapidly in both spatial and temporal dimensions. Though their method is not directly duplicable, it still looks appealing to simplify our PDE with some different approximations that are applicable in the new experimental conditions. This will be the new challenge of further studies.

Appendix A

The aim of this appendix is to calculate $Z_{\rm eff}(Y)$ from the simplified motility model given in Section 2.3. The arbitrary tumbling time distribution in the model is handled by defining a new stochastic process $\boldsymbol{v}'(t')$ to cut all the tumbling periods from the original process $\boldsymbol{v}(t)$. Their relation is given by $\boldsymbol{v}'(t') = \boldsymbol{v}(t)$, where $\mathrm{d}t'/\mathrm{d}t$ is 1 if time t falls in a running period, and is 0 otherwise. Since the model assumes zero displacement during the tumbling periods, the new trajectory is still continuous. This makes such cutting valid.

Cutting all the tumbling periods leads to an important simplification. The new wide-sense stationary process $\boldsymbol{v}'(t')$ has the same parameters $\tau_{\rm run}$, α, and Z_θ as $\boldsymbol{v}(t)$ except that $\tau_{\rm tumble}$ becomes 0. This makes $\boldsymbol{v}'(t')$ Markovian an angular Wiener process due to rotational diffusion interrupted by a Poisson tumbling process. We may then calculate its diffusion constant D' from its second-order moment $\kappa'(\tau) = \langle \boldsymbol{v}'(t')\boldsymbol{v}'(t'+\tau)\rangle$.

The total rotational diffusion angle $\theta_{\rm rot}$ during interval τ is governed by a Gaussian distribution $N(0, 2Z_\theta\tau)$, and thus we have

$$\langle \cos\theta_{\rm rot}\rangle = \int_{-\infty}^{+\infty} \frac{\cos\theta_{\rm rot}}{2\sqrt{\pi Z_\theta \tau}} \times \exp\left(-\frac{\theta_{\rm rot}^2}{4Z_\theta\tau}\right)\mathrm{d}\theta_{\rm rot} = \mathrm{e}^{-Z_\theta\tau}. \quad \text{(A1)}$$

From the independent identical exponential distribution of the running periods, the number n of (instant) tumbles that appear in interval τ in the trimmed process $\boldsymbol{v}'(t')$ follows a Poisson distribution

$$P_n = \frac{1}{n!}\left(\frac{\tau}{\tau_{\rm run}}\right)^n \exp\left(-\frac{\tau}{\tau_{\rm run}}\right), \quad n = 0, 1, \ldots \quad \text{(A2)}$$

The tumbling angles $\theta_1, \theta_2, \ldots, \theta_n$ independently comply with distribution $p(\theta)$ such that $\langle\cos\theta\rangle = \alpha$, according to the model. Therefore, for a given n, the total direction change $\theta_\tau = \theta_1 + \theta_2 + \cdots + \theta_n + \theta_{\rm rot}$ satisfies

$$\begin{aligned}\langle\cos\theta_\tau\rangle_n &= \langle\cos\theta_1\rangle\cdots\langle\cos\theta_n\rangle\langle\cos\theta_{\rm rot}\rangle \\ &= \alpha^n\,{\rm e}^{-Z_\theta\tau},\end{aligned} \tag{A3}$$

where the factorization can be proved from the symmetric distributions of the $n+1$ independent angles. From Eqs. (A2) and (A3), we have

$$\begin{aligned}\kappa'(\tau) &= \langle\boldsymbol{v}'(t')\cdot\boldsymbol{v}'(t'+\tau)\rangle = \sum_{n=0}^{\infty} v^2\langle\cos\theta_\tau\rangle_n P_n \\ &= v^2\,{\rm e}^{-Z_\theta\tau}\sum_{n=0}^{\infty}\frac{1}{n!}\left(\frac{\alpha\tau}{\tau_{\rm run}}\right)^n\exp\left(-\frac{\tau}{\tau_{\rm run}}\right) \\ &= v^2\exp\left[-\left(Z_\theta+\frac{1-\alpha}{\tau_{\rm run}}\right)\tau\right],\end{aligned} \tag{A4}$$

and the diffusion constant is given by

$$D' = \frac{1}{2}\int_0^{+\infty}\kappa'(\tau)\,{\rm d}\tau = \frac{v^2}{2\left(Z_\theta+\dfrac{1-\alpha}{\tau_{\rm run}}\right)}. \tag{A5}$$

Now we put back the tumbling periods. Since $\boldsymbol{v}'(t') = \boldsymbol{v}(t)$ and the cell does not move when tumbling, the total displacement satisfies $\boldsymbol{r}'(t') = \boldsymbol{r}(t)$. Therefore, the diffusion constant of the untrimmed process $\boldsymbol{v}(t)$ is given by

$$\begin{aligned}D &= \lim_{t\to\infty}\frac{\langle r^2(t)\rangle}{4t} = \lim_{t\to\infty}\frac{t'}{t}\lim_{t'\to\infty}\frac{\langle r'^2(t')\rangle}{4t'} \\ &= D'\lim_{t\to\infty}\frac{t'}{t}.\end{aligned} \tag{A6}$$

Note that the following equation holds for arbitrary tumbling time distribution

$$\lim_{t\to\infty}\frac{t'}{t} = \frac{\tau_{\rm run}}{\tau_{\rm run}+\tau_{\rm tumble}}, \tag{A7}$$

only if sufficiently many run-tumble switches occur during time t. The rigorous math involves convergence in probability, which is proved using the law of large numbers.

By comparing Eqs. (A5)–(A7) with Eq. (7), we finally obtain

$$Z_{\rm eff} = \left(\frac{1-\alpha}{\tau_{\rm run}}+Z_\theta\right)\left(1+\frac{\tau_{\rm tumble}}{\tau_{\rm run}}\right). \tag{A8}$$

All the model parameters $\tau_{\rm run}(Y)$, $\tau_{\rm tumble}(Y)$, and $\alpha(Y)$ depend on the CheYp level, but all the above derivation is done at a fixed $Y(c,m)$ level.

Appendix B

This appendix proves our model's compatibility with the K–S equation. Specifically, by taking the frequent tumbling limit at constant diffusion coefficient and then the rapid methylation limit to ensure instant gradient sensing, we obtain the K–S equation from our PDE. As there are two limit processes to happen in succession, the derivation has two steps.

Step 1 Taking the frequent tumbling limit (diffusion limit). In a predefined 2D concentration field $c(\boldsymbol{r},t)$, our PDE (Eq. (8)) reads

$$\begin{aligned}&\frac{\partial P}{\partial t}+\frac{\partial}{\partial m}\left[\dot m(\boldsymbol{r},m,t)P\right]+\boldsymbol{v}(\theta_v)\cdot\boldsymbol{\nabla}P \\ &= Z_{\rm eff}(\boldsymbol{r},m,t)\frac{\partial^2 P}{\partial\theta_v^2},\end{aligned} \tag{B1}$$

where $\boldsymbol{v}(\theta_v) = v\boldsymbol{e}_x\cos\theta_v + v\boldsymbol{e}_y\sin\theta_v$, and v is the maximum swimming speed.

The limit process involves magnifying $Z_{\rm eff}$ uniformly by N times and v by $\sqrt{N}$ times in compensation to keep the diffusion coefficient (see Eq. (7)) constant. In detail, we let $Z_{\rm eff} = Nz$ and $v = \sqrt{N}v'$. We keep z and v' constant and let $N\to\infty$, then equation (B1) is rewritten as

$$\frac{\partial P}{\partial t}+\frac{\partial}{\partial m}(\dot m P)+\sqrt{N}\boldsymbol{v}'(\theta_v)\cdot\boldsymbol{\nabla}P = Nz\frac{\partial^2 P}{\partial\theta_v^2}, \tag{B2}$$

where $\boldsymbol{v}'(\theta_v) = v'\boldsymbol{e}_x\cos\theta_v + v'\boldsymbol{e}_y\sin\theta_v = \boldsymbol{v}(\theta_v)/\sqrt{N}$. Then, we use the following expansion:

$$P = \frac{1}{2\pi}p(\boldsymbol{r},m,t)+\frac{1}{\sqrt{N}}P_1+\frac{1}{N}P_2+o\left(\frac{1}{N}\right), \tag{B3}$$

where $p(\boldsymbol{r},m,t) = \displaystyle\int_0^{2\pi}P\,{\rm d}\theta_v$, since we expect the high tumbling frequency is expected to make P almost uniform in θ_v so that variation is only in the higher order terms.

Substituting the expansion into the rewritten PDE (B2), we obtain

$$\begin{aligned}&\frac{1}{2\pi}\frac{\partial p}{\partial t}+\frac{1}{2\pi}\frac{\partial}{\partial m}(\dot m p)+\frac{\sqrt{N}}{2\pi}\boldsymbol{v}'(\theta_v) \\ &\cdot\boldsymbol{\nabla}p+\boldsymbol{v}'(\theta_v)\cdot\boldsymbol{\nabla}P_1 \\ &= \sqrt{N}z\frac{\partial^2 P_1}{\partial\theta_v^2}+z\frac{\partial^2 P_2}{\partial\theta_v^2}+o(1).\end{aligned}$$

Comparing the terms in the same order of N, we have

$$\frac{1}{2\pi}\boldsymbol{v}'(\theta_v)\cdot\boldsymbol{\nabla}p = z\frac{\partial^2 P_1}{\partial\theta_v^2}, \tag{B4(a)}$$

$$\frac{1}{2\pi}\frac{\partial p}{\partial t}+\frac{1}{2\pi}\frac{\partial}{\partial m}(\dot{m}p)+\boldsymbol{v}'(\theta_v)\cdot\boldsymbol{\nabla}P_1=z\frac{\partial^2 P_2}{\partial\theta_v^2}. \tag{B4(b)}$$

After integrating Eq. (B4(b)) with respect to θ_v in the range of $[0,\ 2\pi]$, we obtain

$$\begin{aligned}&\frac{\partial p}{\partial t}+\frac{\partial}{\partial m}(\dot{m}p)+\boldsymbol{\nabla}\cdot\int_0^{2\pi}\boldsymbol{v}'(\theta_v)P_1 d\theta_v\\&=z(\boldsymbol{r},m,t)\left.\frac{\partial P_2}{\partial\theta_v}\right|_0^{2\pi}=0.\end{aligned} \tag{B5}$$

Now we have to calculate the remaining integral in Eq. (B5) with the help of Eq. (B4(a)). This is done by using the following equation and then integrating by parts twice

$$\begin{aligned}\int_0^{2\pi}\boldsymbol{v}'(\theta_v)P_1\,\mathrm{d}\theta_v&=-\int_0^{2\pi}P_1\frac{\partial^2}{\partial\theta_v^2}\boldsymbol{v}'(\theta_v)\,\mathrm{d}\theta_v\\&=-\int_0^{2\pi}\boldsymbol{v}'(\theta_v)\frac{\partial^2 P_1}{\partial\theta_v^2}\,\mathrm{d}\theta_v\\&=-\frac{1}{2\pi z}\int_0^{2\pi}\boldsymbol{v}'\boldsymbol{v}'(\theta_v)\,\mathrm{d}\theta_v\cdot\boldsymbol{\nabla}p\\&=-\frac{v'^2}{2z}\boldsymbol{I}\cdot\boldsymbol{\nabla}p=-\frac{v'^2}{2z}\boldsymbol{\nabla}p.\end{aligned} \tag{B6}$$

Hence, substituting Eq. (B6) into Eq. (B5), we have

$$\frac{\partial p}{\partial t}+\frac{\partial}{\partial m}(\dot{m}p)=\boldsymbol{\nabla}\cdot\left(\frac{v'^2}{2z}\boldsymbol{\nabla}p\right)=\boldsymbol{\nabla}\cdot\left(\frac{v^2}{2Z_{\mathrm{eff}}}\boldsymbol{\nabla}p\right). \tag{B7}$$

Note that $v^2/2Z_{\mathrm{eff}}$ is precisely the diffusion coefficient $D(Y(c,m))$ in Eq. (7) that remains unchanged in the limit process, then we have

$$\frac{\partial p}{\partial t}+\frac{\partial}{\partial m}\left[\dot{m}(c,m)p\right]=\boldsymbol{\nabla}\cdot\left[D(c,m)\boldsymbol{\nabla}p\right]. \tag{B8}$$

This equation is one dimension lower than our original PDE because the limit process makes P almost homogeneous in θ_v so that after integration θ_v is cancelled from the coordinate list.

Step 2 Taking the rapid methylation limit. This step is more straightforward because this limit process is in itself complete without anything else going on in compensation. We directly let $\dot{m}(c(\boldsymbol{r},t),m)$ be uniformly magnified by N times where $N\to\infty$. This eventually lets the distribution in m converge to the fixed point $m_0(c(\boldsymbol{r},t))$ of the one-dimensional dynamical system. Thus we have

$$p(\boldsymbol{r},m,t)=b(\boldsymbol{r},t)\delta[m-m_0(\boldsymbol{r},t)], \tag{B9}$$

where $b(\boldsymbol{r},t)=\displaystyle\int_{-\infty}^{+\infty}p(\boldsymbol{r},m,t)\,\mathrm{d}m$ is the cell density.

Substituting Eq. (B9) into Eq. (B8), and then integrating it with respect to m, we obtain

$$\begin{aligned}\frac{\partial b}{\partial t}&=\boldsymbol{\nabla}\cdot\left[\left(\int_{-\infty}^{+\infty}D(c,m)\delta(m-m_0)\,\mathrm{d}m\right)\ \boldsymbol{\nabla}b\right]\\&\quad-\boldsymbol{\nabla}\cdot\left[\left(\int_{-\infty}^{+\infty}D(c,m)\delta'(m-m_0)\,\mathrm{d}m\right)\ b\boldsymbol{\nabla}m_0\right]\\&=\boldsymbol{\nabla}\cdot\left[D\left(c,m_0(c)\right)\boldsymbol{\nabla}b\right]+\boldsymbol{\nabla}\\&\quad\cdot\left[\left.\frac{\partial D}{\partial m}\right|_{(c,m_0(c))}m_0'(c)b(\boldsymbol{r},t)\boldsymbol{\nabla}c\right],\end{aligned} \tag{B10}$$

which is exactly the K–S equation. Comparing with Eq. (1), we have from precise adaptation that

$$\mu(c)=D\left(c,m_0(c)\right)=\mathrm{const}, \tag{B11(a)}$$

$$\chi(c)=-\left.\frac{\partial D}{\partial m}\right|_{(c,m_0(c))},$$

$$m_0'(c)=\left.\frac{\partial D}{\partial c}\right|_{(c,m_0(c))}. \tag{B11(b)}$$

Note that Eq. (B11(a)) was exactly the assumption made by many early studies on the K–S equation before the precise adaptation was understood. Now with precise adaptation, we are able to derive not only the K–S equation, but also this fact from our model PDE.

Appendix C

This appendix proves that the K–S equation cannot explain the negative chemotaxis observed in the oscillating concentration field. First, let us rewrite Eq. (1) in the special case of $c=c(x,\ t)$, a 1D field. With precise adaptation, the equation reduces to

$$\frac{\partial p}{\partial t}=-\frac{\partial}{\partial x}\left(p\chi(c)\frac{\partial c}{\partial x}\right)+\mu\frac{\partial^2 p}{\partial x^2}. \tag{C1}$$

Since the two boundaries are idealistically reflective with no additional effects (such as adsorbing bacteria) other than blocking the probability flow, the boundary conditions of the finite microfluidic tube $[a,\ b]$ can be written as

$$p\chi(c)\frac{\partial c}{\partial x}=\mu\frac{\partial p}{\partial x},\quad x=a,b. \tag{C2}$$

Within the finite tube $[a,\ b]$, the center of mass $x_{\mathrm{c}}(t)$ is determined by

$$x_{\mathrm{c}}(t)=\int_a^b xp(x,t)\,\mathrm{d}x, \tag{C3}$$

then the centroid velocity is

$$\frac{\mathrm{d}x_{\mathrm{c}}}{\mathrm{d}t}=\int_a^b x\frac{\partial p}{\partial t}\,\mathrm{d}x$$

$$
\begin{aligned}
&= -\int_a^b x\frac{\partial}{\partial x}\left(p\chi(c)\frac{\partial c}{\partial x}\right)\mathrm{d}x + \mu\int_a^b x\frac{\partial^2 p}{\partial x^2}\mathrm{d}x \\
&= x\left[\mu\frac{\partial p}{\partial x} - p\chi(c)\frac{\partial c}{\partial x}\right]\Bigg|_a^b \\
&\quad + \int_a^b p\chi(c)\frac{\partial c}{\partial x}\mathrm{d}x - \mu p\Big|_a^b \\
&= \int_a^b p\chi(c)\frac{\partial c}{\partial x}\mathrm{d}x - \mu\left[p(b) - p(a)\right]. \qquad \text{(C4)}
\end{aligned}
$$

On the right-hand side of Eq. (C4) there are two terms. The first term results from the gradient while the second term comes from the reflective boundaries. In case of a chemoattractant field ($\chi(c) > 0$), every time the gradient $\partial c/\partial x$ drops to zero cancelling the first term, since $\chi(c)>0$ for chemoattractants, we still have $p(b)> p(a)$ at this moment, because bacteria need time to evacuate from one end to the other. However, from Eq. (C4) we find that this already makes $\mathrm{d}x_\mathrm{c}/\mathrm{d}t < 0$. Therefore, according to the K–S equation, the zero centroid velocity always precedes zero gradient. In other words, the phase of the former should always lead over, rather than lag behind that of the latter no matter how high the oscillation frequency $1/T$ is. The negative chemotaxis due to phase lag is therefore impossible for the K–S equation to account for.

References

[1] Tindall M J, Porter S L, Maini P K, Gaglia G and Armitage J P 2008 *Bull. Math. Biol.* **70** 1525

[2] Ahmed T and Stocker R 2008 *Biophys. J.* **95** 4481

[3] Kalinin Y V, Jiang L, Tu Y and Wu M 2009 *Biophys. J.* **96** 2439

[4] Amarie D, Glazier J A and Jacobson S C 2007 *Anal. Chem.* **79** 9471

[5] Zhu X, Si G, Deng N, Ouyang Q, Wu T, He Z, Jiang L, Luo C and Tu Y 2012 *Phys. Rev. Lett.* **108** 128101

[6] Keller E and Segel L 1971 *J. Theor. Biol.* **30** 225

[7] Tindall M J, Maini P K, Porter S L and Armitage J P 2008 *Bull. Math. Biol.* **70** 1570

[8] Macnab R M and Koshland D E 1972 *Proc. Natl. Acad. Sci.* **69** 2509

[9] Segall J E, Block S M and Berg H C 1986 *Proc. Natl. Acad. Sci.* **83** 8987

[10] Shimizu T S, Tu Y and Berg H C 2010 *Mol. Syst. Biol.* **6** 382

[11] Alon U, Surette M G, Barkai N and Leibler S 1999 *Nature* **397** 168

[12] Stewart R C, Jahreis K and Parkinson J S 2000 *Biochemistry* **39** 13157

[13] Cluzel P, Surette M and Leibler S 2000 *Science* **287** 1652

[14] Turner L, Ryu W S and Berg H C 2000 *J. Bact.* **182** 2793

[15] Schnitzer M J 1993 *Phys. Rev.* E **48** 2553

[16] Alt W 1980 *J. Math. Biol.* **9** 147

[17] Berg H C and Brown D A 1972 *Nature* **239** 500

[18] Vladimirov N, Lebiedz D and Sourjik V 2010 *PLoS Comput. Biol.* **6** e1000717

[19] Vladimirov N, Løvdok L, Lebiedz D and Sourjik V 2008 *PLoS Comput. Biol.* **4** e1000242

[20] Jiang L, Ouyang Q and Tu Y 2010 *PLoS Comput. Biol.* **6** e1000735

[21] Vladimirov N 2009 *Multiscale Modeling of Bacterial Chemotaxis* (Ph. D. Dissertation) (Germany: the Ruperto-Carola University of Heidelberg)

[22] Erban R and Othmer H G 2004 *SIAM J. Appl. Math.* **65** 361